Sedimentation of large particles in a suspension of colloidal rods

B. Barabé,[1, 2, 3, a)] S. Abakumov,[4] D. Z. Gunes,[1] and M. P. Lettinga[2, 5, b)]
[1)]*Nestec Ltd, Société des Produits Nestlé SA, P.O. Box 44 CH-1000 Lausanne 26, Switzerland.*
[2)]*IBI-4, Forschungzentrum Jülich, Wilhelm Jonen Strasse, 52428 Jülich, Germany.*
[3)]*Laboratory for Soft Matter and Biophysics, KU Leuven,Celestijnenlaan 200D, B-3001 Leuven Belgium.*
[4)]*Laboratory for Molecular Imaging and Photonics, KU Leuven, Celestijnenlaan 200F, B-3001, Leuven, Belgium.*
[5)]*Laboratory for Soft Matter and Biophysics, KU Leuven, Celestijnenlaan 200D, B-3001, Leuven Belgium.*

(Dated: 16 April 2020)

The sedimentation at low Reynolds numbers of large, non-interacting spherical inclusions in networks of model monodisperse, slender colloidal rods is investigated. The influence of rod concentration, rod length, and inclusion stress on the inclusion's creeping motion is investigated. The decrease of sedimentation speeds as a function of rod concentration is compared to the Stokes law, using the zero-shear viscosity from the Doi-Edwards theory for semi-dilute colloidal rods solutions. The experimental speeds display the same concentration dependence as the zero-shear viscosity, and are thus strongly dependent on the rod length. The speed is, however, a fraction of 2 and 4 lower than expected for rods of 0.88 and 2.1 μm, respectively. The results for both rod lengths superimpose when plotted against the overlap concentration, hinting at an extra dependence on the entanglement.

I. INTRODUCTION

Suspensions of non-colloidal inclusions in a flowable continuous phase are omnipresent in industrial applications, ranging from consumer products[1,2] to building materials,[3–5] and geological materials such as lava and mud.[6,7] The viscosity profile of the continuous phase enables them to bear the mass of fillers for long shelf life.[8] In the case of structural materials such as cement, fillers are added to tune the visco-elastic properties.[5] As for food products, fat droplets of targeted size stabilized in high viscosity water based matrices, enable the obtention and tuning of specific mouthfeel.[1]

Over long shelf life, unwanted heterogeneities may appear in the products, as gravity induces sedimentation or creaming of solid fillers, bubbles or droplets,[9] resulting in altered end properties.[10] Prediction of particle sedimentation in weak gels is needed to predict product stability over long shelf life. Assessing the stability of systems with solid inclusions in high viscosity fluids is an issue of both industrial applications[1,3–5,8,11] and fundamental relevance.[8,12,13] The ability of a matrix to stabilize inclusions over a long period of time, indeed relates to the existence of a real or apparent yield stress.[13,14]

Most of the theoretical and experimental work performed on hard spherical inclusions in yield stress fluids was dedicated to the following purpose: establishing a macroscopic stability criterion to predict stability and flow. In finite elements numerical simulations, Beris and coworkers[14] studied the creeping motion of inclusions through unbounded Bingham fluids. They showed that inclusion stability can be predicted, using macroscopic quantities such as the inclusion diameter, density mismatch and the matrix yield stress. A dimensionless yield number is obtained, that is a descriptor of the system's stability versus sedimentation taking the ratio of the buoyancy force exerted to the inclusion to the yield force. Below a critical value, the inclusion is heavy enough to yield a region of fluid around it, such that creeping through the fluid is thus possible.[14] The validity of this criterion in the presence of wall effects was assessed for cylindrically bounded Bingham[15] and Herschel-Bulkley fluids,[16] both using the Papanastasiou[17] constitutive equation to solve discontinuity between the solid and liquid region. Experimental assessment of the stability of spherical inclusions in Carbopol suspensions, modeled as Herschel-Bulkley fluids, confirmed the value of the dimensionless yield number.[10,18,19]

As the process of yielding is an interplay between microscopic changes in the material surrounding the inclusion[20] and the sedimentation force exerted by the inclusion,[13,14] it is of interest to have a full understanding of this process. In this paper we report an experimental study of sedimentation speeds of large non-interacting spherical inclusions in a suspension composed of colloidal rods, considered as ideal. We show that using ideal colloidal rods as host medium facilitates comparison between theory and experiments, as the rheological behavior of rods suspensions is by now well described by theory.[21] In principle these systems do not show a yielding behavior, while the zero-shear viscosity hugely depends on length and concentration of the rods.

However, a yielding-like behavior of inclusions in highly concentrated dispersions of anisotropic particles cannot be excluded. Sedimentation studies of inclusions in yield stress fluids composed of anisotropic particles were performed on, amongst others, cellulose suspensions,[22,23] castor oil colloidal fibers in a surfactant suspension,[24] laponite suspensions,[25,26] viscoelastic polysaccharide solutions[27,28] and wormlike micellar fluids.[12,29,30] The latter do not possess true yield stresses, but only an apparent yield stress when excited above the characteristic relaxation time of the matrix. Characteristic features of inclusions falling in shear-thinning fluids were evidenced. For several of those shear-thinning fluids, negative

[a)]Electronic mail: Blandine.Barabe@kuleuven.be
[b)]Electronic mail: p.lettinga@fz-juelich.de

wake was reported,[12,25] which is local flow in the direction opposite to sedimentation in the inclusions' wake. It is associated to a fluid's increase in viscoelasticity[26] and has an increased geometrical span for high extensional Deborah and Reynolds numbers.[12,27] For high extensional Deborah numbers, spheres and bubbles sedimenting in wormlike micellar fluids are found never to reach a terminal speed and oscillate in the direction along the gravity axis, amongst other reported effects.[12] Additionally, inclusions chaining was reported for shear-thinning viscoelastic fluids such as xanthan, below a critical distance between closest neighbours.[27,31]

The scope of our study is to stay in the creeping motion domain for non-interacting inclusions at Reynolds numbers lower than 10^{-6}. For the model systems considered only a classical monotonic sedimentation behavior is expected, excluding negative wake, oscillatory settling and particles chaining effects. We consider a model composed of the simplest anisotropic particles: suspensions of slender colloidal rods. Fd and pf1 virus bacteriophages[32] are the best suited[33,34] for this study, because they are very slender and monodisperse by nature, differing about a factor two in length. They provide an exact interbatch reproducibility, while their rheological behavior has been well characterized.[21] These colloidal rods are density matched with their dispersing solvent and can be produced in high quantities. The rods' electrostatic interactions are tunable[32] and they display an isotropic to nematic transition at well characterized concentrations. Fd virus has been used for studying the diffusion of spherical inclusions through isotropic rod networks[35,36] and the phase behavior of rod-sphere mixtures;[32,35–37] the size of the inclusions was of the order of the length of fd or smaller, so that the fd matrix could not be considered as a continuum with regards to the inclusion. The ideal character of the system allows us to study the effect of concentration. Concentration effects have been reported earlier[24,28], however, the used systems are not straightforward to model.

In this paper, the dependence of the sedimentation speed on inclusion stress is investigated in the semi-dilute regime for two different rod lengths at least five times smaller than the inclusions. We address the question whether this system possesses an apparent yield stress behavior, which would arrest sedimentation at low inclusion stress and whether the sedimentation speed can be understood on the base of the known rheological behavior of the host system.

II. THEORY

In this theory section, we first introduce the characteristic numbers and equations associated to the sedimentation of a rigid, spherical inclusion in an unbounded, unknown matrix. Then, the equation for the sedimentation of an inclusion in creeping flow conditions will be specified for a matrix that is a colloidal suspension of rods.

The buoyancy force of the inclusion is non-zero when there is a density mismatch with the suspending fluid. The inclusion falls down or rises in the matrix with an average sedimentation speed V_S and induces an average shear rate $\dot{\gamma}$. The latter is usually expressed[12,25] as the ratio of the average sedimentation speed by the diameter of the inclusion:

$$\dot{\gamma} = \frac{V_S}{2\,R}, \tag{1}$$

where V_S is the terminal speed that is reached after establishment of a steady-state of sedimentation dynamics, averaged over all inclusions, of diameter R.

The stress τ_I exerted by the inclusion on the surrounding matrix is then expressed as:

$$\tau_I = \frac{F_I}{S} = \frac{2}{3}\,R\,g\,\Delta\rho, \tag{2}$$

where F_I is the inclusion buoyancy force exerted on the surface S. $\Delta\rho$ is the density mismatch and g the gravitational constant.

The terminal speed of a spherical inclusion in an unbounded viscous fluid is expressed using the Stokes law:

$$V_t = \frac{2}{9}\,\frac{\Delta\rho}{\eta_m(\dot{\gamma})}\,g\,R^2. \tag{3}$$

$\eta_m(\dot{\gamma})$ is the shear rate dependent viscosity of the matrix. Using (2), the terminal speed can be expressed as a function of the inclusion stress:

$$V_t = \frac{1}{3}\,\tau_I\,\frac{R}{\eta_m(\dot{\gamma})}. \tag{4}$$

In Newtonian fluids, $\eta_m(\dot{\gamma})$ is a constant. However, in non-Newtonian fluids $\eta_m(\dot{\gamma})$ strongly depends on the shear rate. In the case of semi-dilute colloidal rods for example, the viscosity strongly decreases with increasing shear rate. Moreover, for suspensions of colloidal rods, viscosity increases with rod concentration. In the particular case of our system, we assess the shear-rate and concentration dependance of viscosity. For the stresses used in this work, the resulting sedimentation rates will be so low that we only need to take the zero-shear viscosity into consideration, as we will show later in the paper. The zero-shear viscosity strongly depends on concentration as well as length, as has been recently shown for fd and pf1.[21] Based on the Doi-Edwards theory and the zero-shear viscosity is given by[21] as

$$\eta_m = \eta_S\left[1 + \nu\,\frac{\pi L^3}{90\,ln(\frac{L}{2d})} + \nu^3\,\frac{\pi L^9}{30\,K\,ln(\frac{L}{2d})}\right]. \tag{5}$$

L and d are the length and diameter of a colloidal rod. ν is the colloidal rods' number density, η_S the solvent viscosity. K is a proportionality constant that is best determined by rheology.[21] For stiff rods we use the computed and experimentally validated Teraoka value, K = 1300. The experimental value of K = 2300 accounts for the relatively higher flexibility of pf1. In the zero-shear viscosity equation, the first term corresponds to the contribution of the solvent viscosity. The second term is the contribution of rotational diffusion of non-interacting rods to the viscosity. The third term takes into account the constrained rotational diffusion of a colloidal rod in the semi-dilute case. As one can see, there is a strong dependence of the zero-shear viscosity with the number density and thus, with rod concentration, and a even more pronounced dependence on the rod length.

Using the zero-shear viscosity from the Doi-Edwards theory in the Stokes terminal speed expression, a predictive expression for the inclusion's terminal speed can be derived. This will be further referred to as the Stokes Doi Edwards (SDE) prediction:

$$V_t(\nu) = \frac{1}{3}\,\tau_I\frac{R}{\eta_S\left[1 + \nu\,\frac{\pi L^3}{90\,ln(\frac{L}{2d})} + \nu^3\,\frac{\pi L^9}{30\,K\,ln(\frac{L}{2d})}\right]}. \tag{6}$$

III. MATERIALS

A. Rods suspension.

Fd and pf1 are bacteriophages composed of a DNA single strand coated with a protein layer. They are negatively charged in the dispersing solvent at pH 8.15 and ionic strength 10 mM. Fd virus has a molecular weight of $M_W = 1.64\times 10^7$ g/mol, a contour length of $L = 880$ nm, a persistence length of $L_P = 2200$ nm and a diameter of $D_{bare} = 6.6$ nm. Fd was grown at the Forschungzentrum Jülich following a protocol as are described elsewhere.[35] Pf1 has a molecular weight of $M_W = 3.75\times 10^7$ g/mol, a contour length of $L = 2\ \mu$m, $L_P = 2.2\ \mu$m and diameter $D_{bare} = 6.6$ nm. Pf1 phage was bought from Asla Biotech, Latvia. Viruses were dispersed in a 20 mM tris-HCl buffer at pH 8.15, which corresponds to an ionic strength of 10 mM. In the paper, we use mass concentration, which is linked to number densities by $c = \nu M_w/N_a$, and also scaling with the overlap concentration $c^* = 3M_w/4\pi N_a(\frac{L}{2})^3$, which is 0.076 mg/mL for fd and 0.013 mg/mL for pf1. We focus on semi-dilute suspensions of rods, between $10\times c^*$ and the isotropic-nematic transition: from 1 to 9 mg/mL for fd virus and from 0.1 to 3 mg/mL for pf1. Virus concentrations were determined by UV-visible spectrometry using a Varian Cary® 50 UV-Vis Spectrophotometer, and NanoDrop 2000/2000c Spectrophotometer, Thermo Scientific.

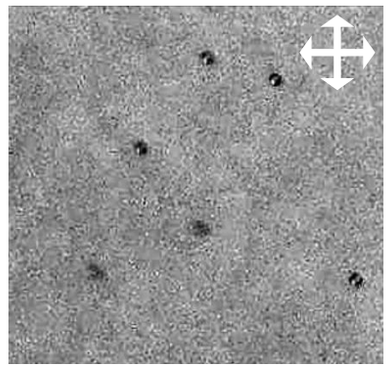

FIG. 1. Birefringence image of sedimenting 10 μm polystyrene spherical inclusions in a pf1 virus solution at c(pf1) = 2.8 mg/mL, inclusion stress of 1.6 mPa. Although the contrast is enhanced, and light intensity maximized in crossed polarized configuration, no birefringence around the falling inclusions is observed.

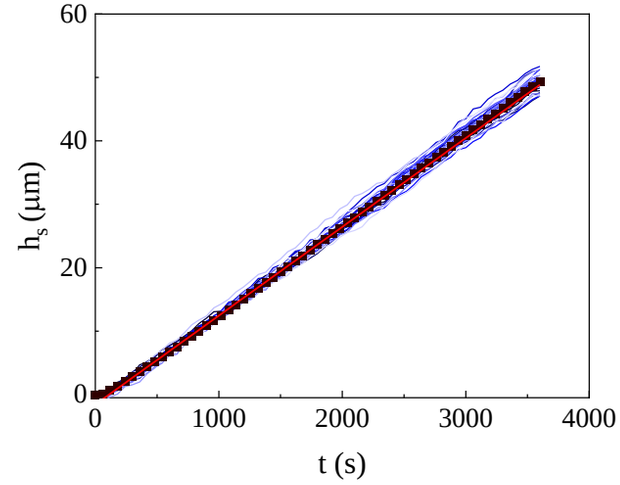

FIG. 2. The sedimentation height h_S of the inclusions as a function of time. Blue lines: trajectories in the sedimentation direction extracted from the timelapse images of polystyrene inclusions in fd virus suspensions, post filtering using a speed histogram; scatter: average trace; red line: linear regression of the average trace. The sample characteristics are: c = 7 mg/mL, I = 10 mM, τ_I = 1.6 mPa.

B. Inclusions.

Polystyrene spherical inclusions were purchased from Polysciences Inc., Polybead® Microspheres. They have a mean diameter of 10.0 μm, with a variance coefficient of 10 %. We determined the density of the beads by tracking their sedimentation speeds V_s in buffers of varying densities. The density is estimated at 1.0494 g/mL, performing an extrapolation to $V_s \to 0$. In order to tune the stress applied by the inclusion on the surrounding matrix, the inclusion's buoyancy was tuned. Buffers of densities ranging from 1.000 g/mL to 1.049 g/mL were prepared by mixing 20 mM Tris-HCl buffer with deuterated water, Acros Organic, giving an ionic strength I = 10 mM. This corresponds to buoyancy forces ranging between F = 0.25 $\times 10^{-12}$ N for the least matched inclusion and 2.05 $\times 10^{-15}$ N for the closest matching in the case of the I = 10nmM water buffer. This corresponds to stresses ranging from 0.0013 to 1.6 mPa, using $\tau = F/S$. The final sample was prepared by vortexing the stock fd virus suspensions, the spherical inclusions suspensions and buffer for approximately one minute. This ensures a random distribution of the inclusions in the sample at t = 0, when the rectangular capillaries of dimensions 2.0 mm $\times$ 0.2 mm were loaded. The volume fraction of beads in the final samples is $\phi_I = 0.07$ % so that we can neglect interactions between the beads.

The mixtures of virus and inclusion are considered to be mixtures of rigid bodies, as used earlier in the study of the phase diagram of rod-sphere mixtures[37]. Flexibility of the rods will, however, affect the results to some extent, as will be discussed below.

C. Imaging.

Sedimentation of inclusions in bacteriophage suspensions was imaged with two set ups: a home-build horizontal microscope based on Olympus components (BX-KMA-ESD imaging revolver), equipped with a Hamamatsu ImagEM X2 EM-CCD camera and a Keyence digital microscope, VHX-6000, equipped with the VHX-S650 free angle observation system, and operating with Keyence software. Both microscopes used a 10 x objective and recorded with a frame rate of 1 image per minute. Fig. 1 displays an image of the inclusions taken between crossed polarizers in order to probe possible birefringence during sedimentation.

The inclusions positions were tracked using the particle-tracking package Trackpy, which is the Python adaptation of the Weeks and Crocker image analysis IDL code.[38] The downwards trajectories h_s of the inclusions are plotted in fig. 2 as a function of the experimental time, t. The trajectories evolve linearly with time as is the case for classical convective sedimentation. Spurious features and trajectories are filtered out. Traces are selected using speed histograms. Outlying lower speeds are filtered out as they correspond to inclusions stuck to the wall or interacting inclusions.[39] The filtered traces are averaged and a linear regression is carried out to extract the average sedimentation speed. The standard deviation of the slope is a measure of the experimental error.

Translational and rotational diffusion coefficients of virus particles in virus suspensions were obtained from mean square displacements and mean square angular displacements. These are obtained from fluorescence microscopy on tracer amounts of fluorescently labeled tracer viruses (Alexa Fluor from ThermoFischer).[40] A Zeiss Axiovert equipped with a 100x NA oil immersion objective, a Prizmatix LED lamp and an Andor sCMOS camera was used for the imaging at frame rates between 10 and 100 fps, depending on the concentration. In order to properly extract the angular diffusion information, a length filter was applied to the traces, so that only particles which diffuse parallel in the plane are tracked. The rotational

diffusion rates, approach the Doi prediction, where D_r is proportional to the scaled number density νL^3, see fig. 3. The pf1 data deviate more as the rod is effectively more flexible.

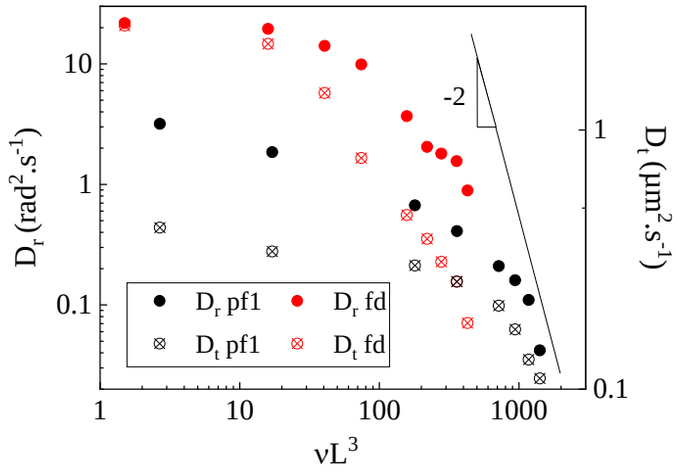

FIG. 3. Rotational and translational diffusion constants for fd and pf1 virus as a function of virus number density time virus length power 3. The diffusion constants stem from fluorescent imaging experiments.

IV. RESULTS

We assessed how inclusion stress, rod concentration and length influence the sedimentation speed. Fig. 4a displays an overlay of absolute sedimentation speeds as a function of inclusion stress for the different considered fd rod concentrations. We performed a linear fit of the increasing sedimentation speed with increasing inclusion stress and compared the resulting slopes $\langle V_S/\tau \rangle$ with the SDE prediction, eq. 6. The results are plotted in fig. 4). This prediction gives the correct functional dependence of $\langle V_S/\tau \rangle$ on the rod concentration. Nevertheless there is a remarkable and unexpected shift of a factor 2.5 between the experimental data and the SDE prediction over the studied concentration range. Note that for the pure solvent the slope corresponds with the Stokes-Einstein prediction.

Fig. 5a displays the reduced sedimentation speed versus the concentration for fd as well as pf1 at a fixed inclusion stress of 1.6 mPa. As expected, a deviation from the SDE prediction for stiff rods is also observed in this representation. It is similar for both rods, but more pronounced for the longer pf1 system than for the shorter fd. Furthermore, the deviation for pf1 is even more pronounced when using the SDE prediction accounting for pf1 flexibility. Again, we can fit the data by correcting the SDE prediction for fd with a factor 2 and the SDE prediction for pf1 with a factor 4, when the rod is considered stiff. The SDE prediction for pf1 accounting for flexibility can be scaled with a factor 7. This scaling is obviously only valid for the high concentrations. The more pronounced slowing down for pf1 is in accordance with eq. 6, which states that the longer rod length will result in an overall

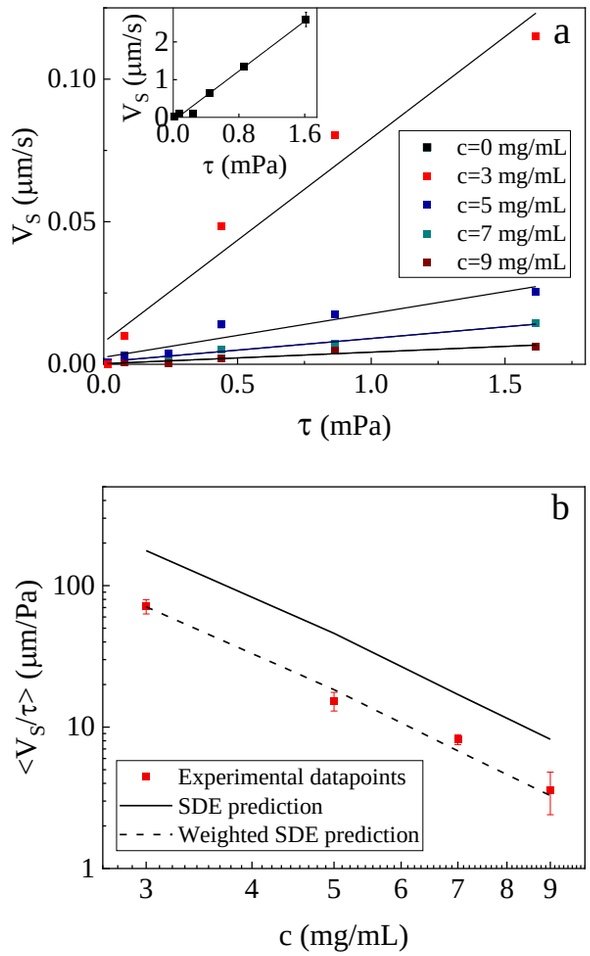

FIG. 4. For fd virus, a) Raw sedimentation speed as a function of inclusion stress, with linear regression. The 0 concentration sedimentation speeds are in the inset. b) Slopes obtained from (a) as a function of concentration. The solid line is the SDE prediction. The dashed lined is the SDE prediction divided by a factor 2.5.

higher viscosity for an undisturbed isotropic network of rods and therefore in slower sedimentation speeds for pf1. In order to take into account the very different overlap concentrations of both systems, we scale the concentration with c^*, see fig. 5b. Surprisingly, the experimental values for pf1 and fd collapse on one master plot.

V. DISCUSSION

The first conclusion we can draw from our experiments is that the existence of an apparent yield stress for dispersions of semi-dilute ideal slender rods cannot be claimed. Indeed, the data shown in fig. 4a in principle all extrapolate to zero. The absence of convective motion for the lowest stress is attributed to the very low density mismatch between the inclusions and the medium. We do observe a substantial slowing down of the sedimentation, which displays the same concentration dependence as predicted by the SDE prediction based

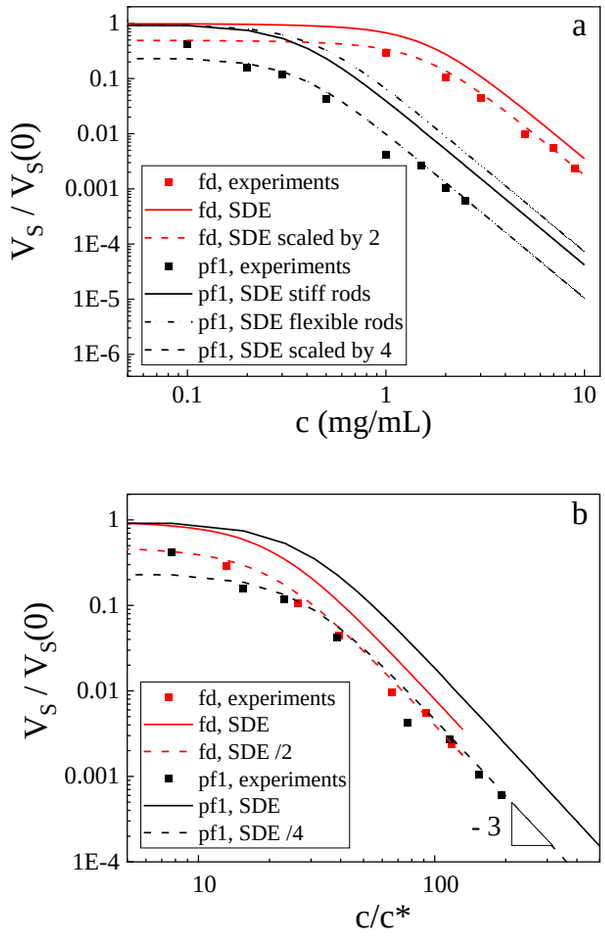

FIG. 5. a) Reduced sedimentation speed for fd and pf1 at an inclusion stress of 1.6 mPa with the SDE prediction in the case of pf1 for two values of K. b) Reduced sedimentation speed as a function of reduced rod concentration c/c *, for both systems fd wild type and pf1.

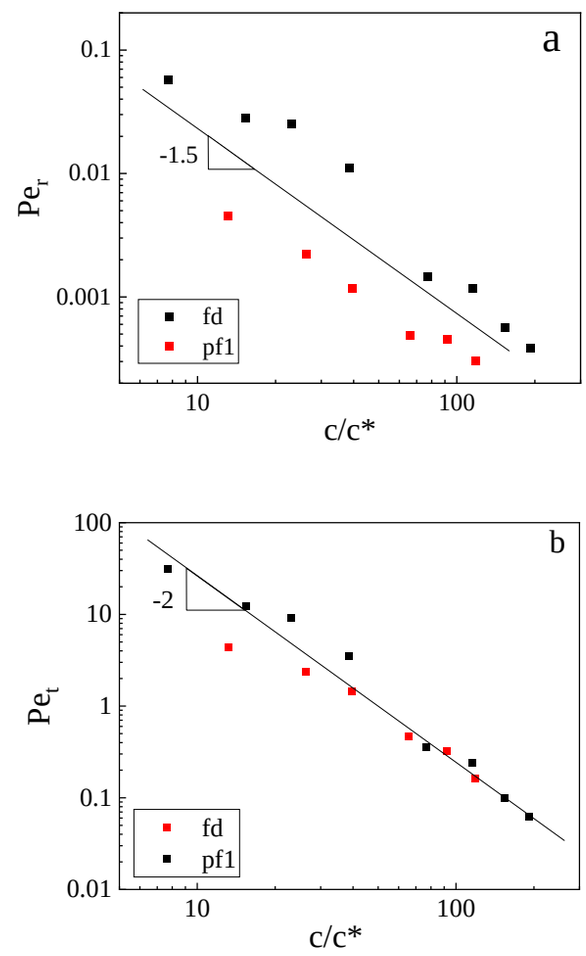

FIG. 6. Rotational (a) and translational (b) Peclet number for fd and pf1 as a function of rod concentration rescaled by c*; the Peclet numbers are calculated using sedimentation rates from experiments. The characteristic diffusion times at the corresponding rod concentrations are extrapolated from 3.

on the rotational relaxation of the rods. However, the SDE underestimates the slowing down by a factor that seems to depend on the rod length.

To interpret the results, we start by validating the assumption that the relevant viscosity is the zero-shear viscosity, see eq. 6. To this end we need to compare the sedimentation-induced shear rate with the relevant relaxation times per system, which is the rotational diffusion in the case of rods. The characteristic sedimentation time is defined as the time needed for an inclusion to fall over a distance of one diameter, $2\,R/V_S = 1/\dot{\gamma}$. For the suspension of colloidal rods, we define a rotational network relaxation time, $1/\,D_r$ where D_r is an experimentally determined rotational diffusion coefficient associated to rods in the semi-dilute regime.[41]

The rotational Peclet number for a spherical inclusion is expressed as follows:[41]

$$Pe_r = \lambda\,\gamma = \frac{V_S}{2\,R\,D_r}. \qquad (7)$$

Fig. 6a displays the experimental rotational Peclet number for fd and pf1 as a function of rod concentration rescaled by c^*. For both rods, the rotational Peclet number is always much smaller than 1, so the sedimentation is slower than network relaxation and no shear thinning takes place for the considered systems, as experimentally confirmed by the absence of birefringence during sedimentation, see fig. 1.[26] This validates the use of the zero-shear viscosity.

The fact that the experimental speeds are smaller than computed from the macroscopic SDE relation rather implies that the inclusions sense a higher viscosity than the zero-shear viscosity obtained from the bulk rheology. Hence, we need to understand whether a local flow-induced shear thickening could develop in front of the inclusion, as opposed to the shear thinning discussed above. In bulk rheology a homogeneous shear flow is exerted on all the probed fluid. In contrast, a falling inclusion exerts an inhomogeneous, localized stress on the medium, so that local microscopic effects around the inclu-

sions need to be considered. Indeed, complex velocity patterns around inclusions were evidenced by particle tracking velocimetry in the vicinity of large inclusions falling in yield stress fluids,[18,26] and for shear-thinning fluids composed of anisotropic-like particles[12,27] in the creeping flow regime. For small inclusions diffusing in fd virus networks, Kang[35,36] assumed a local density variation below (higher rods density in the sedimentation front) and above (lower density in the sedimentation wake) inclusions. This may explain discrepancies between the viscosity in the vicinity of the inclusion, and the one measured with macroscopic rheometry.

We showed above that in our experiments, the sedimentation of the inclusion does not affect the local orientational order. However, it could indeed be that there is a densification in the front of the sedimenting inclusion, which would lead to a higher local viscosity. Such a mechanism has been mentioned for inclusions sedimenting or creaming in cellulose suspensions.[22,23] As the relevant relaxation mechanism for concentration gradients is translational diffusion, we introduce the experimentally defined translational relaxation time. It is defined as the time needed for a rod to translationally diffuse over the diameter of the inclusion, equilibrating local concentration gradients: $(2R)^2/D_\mathrm{t}$, where D_t is the parallel diffusion coefficient associated to rods. The corresponding translational Peclet number is now defined as

$$Pe_\mathrm{t} = \lambda\ \gamma = 2R\,\frac{V_\mathrm{S}}{D_\mathrm{t}} \tag{8}$$

Fig. 6b displays the translational Peclet number for fd and pf1 as a function of the rescaled rod concentration. Over the full concentration range Pe_t is about two orders of magnitude higher than the rotational Pe_r. This does indicate that the translational reorganization is not instantaneous as is the case for the rotational reorganization. We hypothesize that a crowding effect in front of the inclusion is at the origin of the slower sedimentation speed observed, in comparison with the SDE prediction. However, the continuous decrease in Pe_t contradicts the observed constant deviation from SDE, especially at high concentrations. Moreover, at fixed concentrations Pe_t is lower for pf1 than for fd, which cannot explain the larger discrepancy between experimental and theoretical speeds for pf1.

For a deeper understanding, we need to consider the fact that the data for fd and pf1 superimpose when plotted against the concentration scaled with the overlap concentration. This suggests that the sedimentation speed depends on the number of entanglements per rod, which is not the same as the tube diameter that is the base of Doi's theory as reflected in eq. 6. Although the relaxation of entanglements is still correctly described by Doi, given the correct concentration dependence of V_S and results from rheology,[21] there is apparently an extra contribution to the viscosity when dragging an inclusion through an entangled medium. Assuming that there is a densification in front of the falling inclusion, there will be an imbalance in the osmotic pressure between the wake and the front of the inclusion. This imbalance would drive the inclusion in the direction opposite to the sedimentation direction. This extra contribution would be concentration and length dependent. The overlap concentration is also key to explain the increased discrepancy for pf1 between experimental speeds and the SDE prediction when accounting for flexibility. Flexibility causes on the one side a lower macroscopic zero shear viscosity[21] due to the extra relaxation mode, but hardly affects the overlap concentration. On the other side, the sedimenting inclusion is not sensitive to this relaxation, as it does not affect the overlap concentration. This is an important notion, considering the many semi-flexible systems used in applications. When flexibility increases further, the overlap concentration will at some point be affected, as for linear polymers for instance.

VI. CONCLUSION.

Sedimenting, inert spherical inclusions suspended in semi-dilute dispersions of ideal monodisperse rod-like particles, of lengths 0.88 and 2.1 μm, were tracked. The influence of rod concentration, rod length and inclusion stress on the sedimentation speed was investigated. We report a strong decrease of the reduced sedimentation speed as a function of rod concentration, and no apparent yield stress could be identified for the system. Using a theoretical prediction for the zero-shear viscosity of these systems, we find the correct concentration dependence of the sedimentation speed. Hence, the effect of the rod length is very pronounced so that a two-fold increase in the length of the rod slows down the sedimentation speeds by two orders of magnitude at a fixed concentration. The results for both rod lengths superimpose, however, when scaling the concentration with the overlap concentration and there is a constant difference between experiment and theory of a factor 2 and 4 for the shorter and longer rods, respectively. When flexibility is taken into account, the difference with theory is even larger. We infer that crowding in front of the inclusions, causing an increased viscosity, is not sufficiently equilibrated by translational diffusion of the rods. This phenomenon still needs a theoretical underpinning.

CONFLICTS OF INTEREST

There are no conflicts to declare.

SUPPLEMENTARY MATERIAL

supplementary material for the rotational and translational mean square displacements of virus particles at varying concentration.

ACKNOWLEDGEMENTS

This project has received funding from the European Union's Horizon 2020 research and innovation programme under the Marie Sklodowska-Curie Grant Agreement No

641839. The JCNS-PGI workshop, Forschungzentrum Jülich is acknowledged for assistance in design and realization of the capillary holder, and other items on the home-build horizontal microscopic setup. Harmut Kriegs is acknowledged for general discussions on the setup. Karin Sellinghof is acknowledged for the preparation of fd virus suspensions.

NOTES AND REFERENCES

[1]C. Chung and D. J. McClements, Food Structure **1**, 106 (2014), ISSN 22133291.
[2]M. Mehta, N. Shah, and S. Shah, J Pharm Sci Bioscientific Res. pp. 420–426 (2016).
[3]B. L. Damineli, V. M. John, B. Lagerblad, and R. G. Pileggi, Cement and Concrete Research **84**, 8 (2016), ISSN 0008-8846, URL http://dx.doi.org/10.1016/j.cemconres.2016.02.012.
[4]W. She, Y. Du, C. Miao, J. Liu, G. Zhao, and J. Jiang, Cement and Concrete Research (2018).
[5]L. Du and K. J. Folliard, Cement and Concrete Research **35**, 1463 (2005).
[6]A. Tran, M. L. Rudolph, and M. Manga, Journal of Volcanology and Geothermal Research **294**, 11 (2015), ISSN 03770273, URL http://dx.doi.org/10.1016/j.jvolgeores.2015.02.004.
[7]N. Bagdassarov and H. Pinkerton, Journal of Volcanology and Geothermal Research **132**, 115 (2004).
[8]R. P. Chhabra, *Bubbles, Drops, and Particles in Non-Newtonian Fluids* (Taylor & Francis Group, 2007), ISBN 9780824723293.
[9]N. Neirynck, P. Van Der Meeren, S. Gorbe Bayarri, S. Dierckx, and K. Dewettinck, Food Hydrocolloids (2004).
[10]G. Ovarlez, F. Bertrand, P. Coussot, and X. Chateau, Journal of Non-Newtonian Fluid Mechanics **177-178**, 19 (2012), ISSN 03770257, 1206.1505.
[11]M. Mehta, N. Shah, and S. Shah, **6**, 420 (2016).
[12]H. Mohammadigoushki and S. J. Muller, Journal of Rheology **60**, 587 (2016), ISSN 0148-6055, URL http://sor.scitation.org/doi/10.1122/1.4948800.
[13]Y. Holenberg, O. M. Lavrenteva, U. Shavit, and A. Nir, Physical Review E **066301**, 1 (2012).
[14]A. N. Beris, J. A. Tsamopoulos, R. C. Armstrong, and R. A. Brown, Journal of Fluid Mechanics **158**, 219 (1985), ISSN 14697645.
[15]J. Blackery and E. Mitsoulis, J. Non-Newtonian Fluid Mech (1997).
[16]M. Beaulne and E. Mitsoulis, Journal of Non-Newtonian Fluid Mechanics **72**, 55 (1997), ISSN 03770257.
[17]E. Mitsoulis, Rheology Reviews pp. 135–178 (2007).
[18]A. M. Putz, T. I. Burghelea, I. A. Frigaard, and D. M. Martinez, Physics of Fluids **20** (2008), ISSN 10706631.
[19]H. Tabuteau, P. Coussot, and J. R. de Bruyn, Journal of Rheology **51**, 125 (2007), ISSN 0148-6055.
[20]K. N., P. Ballesta, R. Besseling, W. C. K. Poon, and J. F. e. a. Brady, **1518** (2013).
[21]C. Lang, Macromolecules (2019).
[22]H. Emady, M. Caggioni, and P. Spicer, Journal of Rheology **57**, 1761 (2013), ISSN 0148-6055, URL http://sor.scitation.org/doi/10.1122/1.4824471.
[23]C. Song, J., S. M., and T. et al., Rheol Acta **58**, 217–229 (2019), URL https://doi.org/10.1007/s00397-019-01140-4.
[24]S. Mirzaagha, R. Pasquino, E. Iuliano, G. D'Avino, F. Zonfrilli, V. Guida, and N. Grizzuti, Physics of Fluids **29**, 093101 (2019), URL https://doi.org/10.1063/1.4998740.
[25]B. Gueslin, L. Talini, B. Herzhaft, Y. Peysson, and C. Allain, Physics of Fluids **18**, 1 (2006).
[26]B. Gueslin, L. Talini, and Y. Peysson, Rheologica Acta **48**, 961 (2009), ISSN 00354511.
[27]E. Verneuil, R. J. Phillips, and L. Talini, Journal of Rheology **51**, 1343 (2007), ISSN 0148-6055, URL http://sor.scitation.org/doi/10.1122/1.2780799.
[28]M. M. Mrokowska and A. Krztoń-Maziopa, Langmuir **9**, 2104 (2019), URL https://doi.org/10.1038/s41598-019-44233-z.
[29]S. Wu and H. Mohammadigoushki, Journal of Rheology **62**, 1061 (2018), https://doi.org/10.1122/1.5031899, URL https://doi.org/10.1122/1.5031899.
[30]Z. Wang, S. Wang, L. Xu, Y. Dou, and X. Su, Journal of Dispersion Science and Technology **41**, 639 (2020), https://doi.org/10.1080/01932691.2019.1610423, URL https://doi.org/10.1080/01932691.2019.1610423.
[31]S. Daugan, L. Talini, and C. e. a. Herzhaft, Eur. Phys. J. E **9: 55** (2002).
[32]Z. Dogic, J. Zhang, A. W. Lau, H. Aranda-Espinoza, P. Dalhaimer, D. E. Discher, P. A. Janmey, R. D. Kamien, T. C. Lubensky, and A. G. Yodh, Phys Rev Lett **92**, 125503 (2004), ISSN 0031-9007 (Print) 0031-9007 (Linking), URL internal-pdf://162.159.203.92/PRL{_}polymer{_}in{_}nematic.pdfhttps://www.ncbi.nlm.nih.gov/pubmed/15089684.
[33]R. Oldenbourg, X. Wen, R. B. Meyer, and D. L. D. Caspar, Phys. Rev. Lett. **61**, 1851 (1988), URL https://link.aps.org/doi/10.1103/PhysRevLett.61.1851.
[34]A. Zöttl, K. E. Klop, A. Balin, Y. Gao, J. M. Yeomans, and D. G. A. L. Aarts, Soft Matter **15**, 5810 (2019), URL http://dx.doi.org/10.1039/C9SM00903E.
[35]K. Kang, J. Gapinski, M. P. Lettinga, J. Buitenhuis, G. Meier, M. Ratajczyk, J. K. Dhont, and A. Patkowski, J Chem Phys **122**, 44905 (2005), ISSN 0021-9606 (Print) 0021-9606 (Linking), URL internal-pdf://126.198.88.1/Kang05-spheres-crowded.pdfhttps://www.ncbi.nlm.nih.gov/pubmed/15740296.
[36]K. Kang, A. Wilk, J. Buitenhuis, A. Patkowski, and J. K. Dhont, J Chem Phys **124**, 44907 (2006), ISSN 0021-9606 (Print) 0021-9606 (Linking), URL internal-pdf://234.220.117.14/Kang{_}JCP-diffusion2-IN.pdfhttps://www.ncbi.nlm.nih.gov/pubmed/16460212.
[37]D. M. Guu, Ph.D. thesis, Heinrich Heine Universität, Düsseldorf (2014).
[38]D. G. G. John C. Crocker, Journal of colloid and interface science **310**, 298 (1996).
[39]Élisabeth Guazzelli, Comptes Rendus Mécanique **334**, 539 (2006), ISSN 1631-0721, observation, analysis and modelling in complex fluid media, URL http://www.sciencedirect.com/science/article/pii/S1631072106001203.
[40]M. P. Lettinga, J. K. Dhont, Z. Zhang, S. Messlinger, and G. Gompper, Soft Matter **6**, 4556 (2010), ISSN 1744683X.
[41]G. Kumar and G. Natale, Physics of Fluids **31** (2019), URL http://dx.doi.org/10.1063/1.5108749.

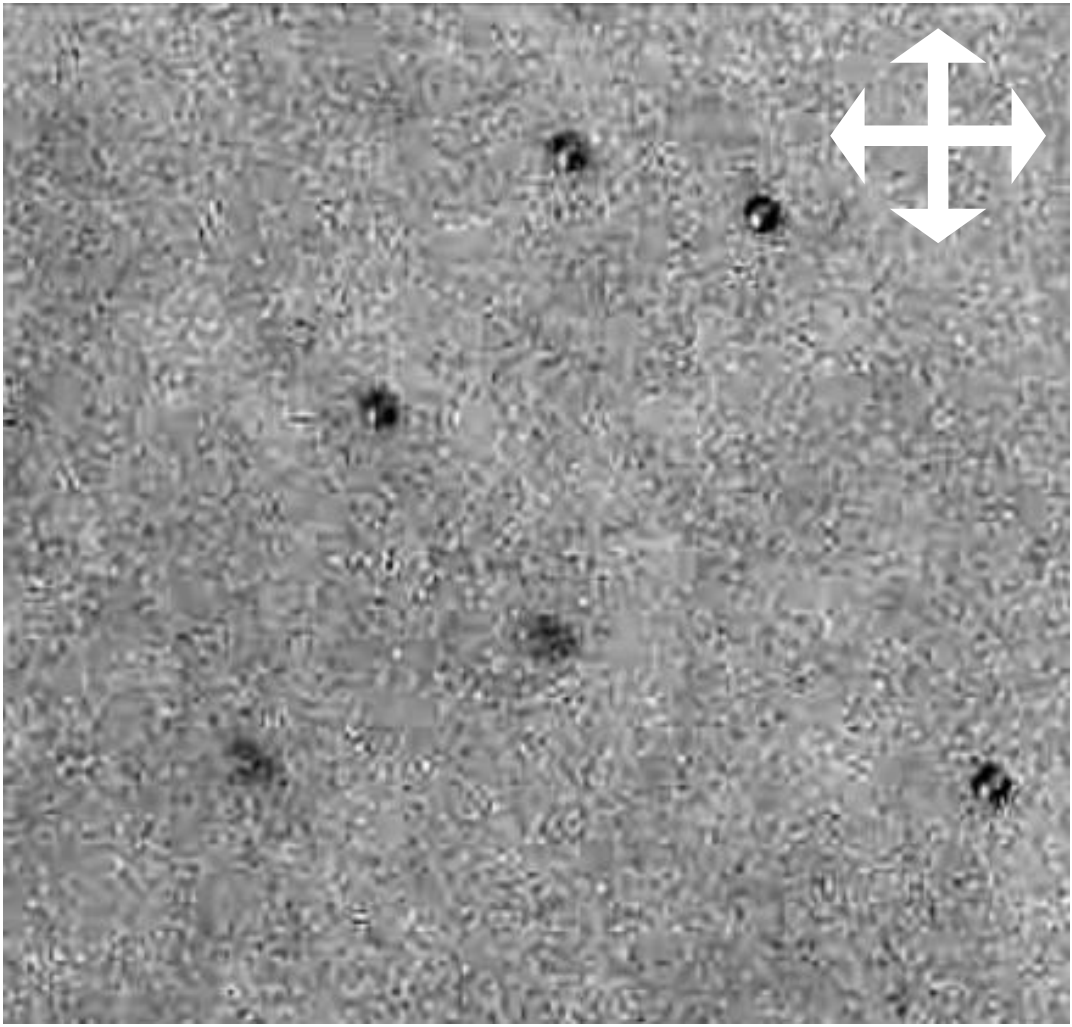

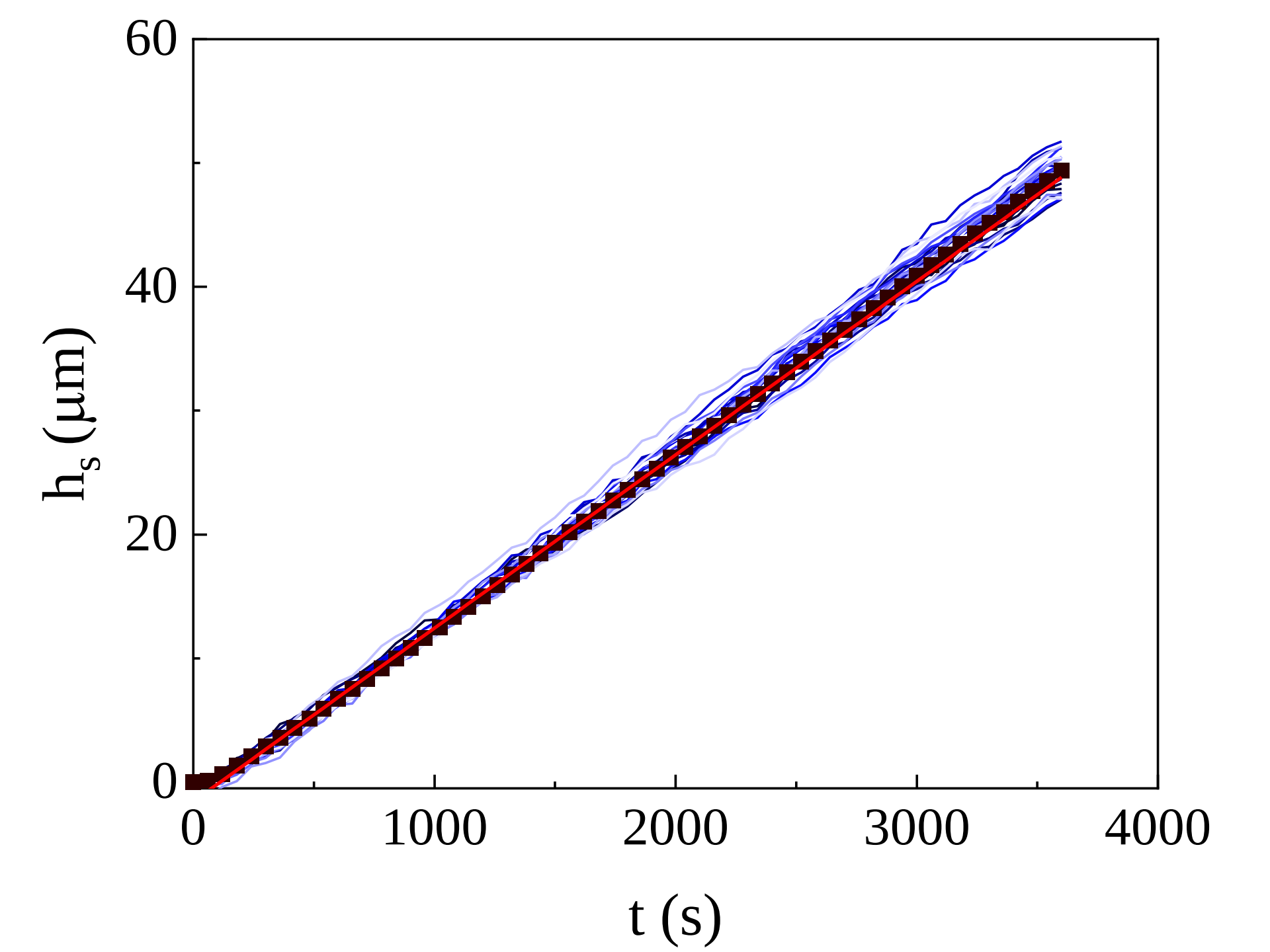
60
40
20
0
h_s (μm)
0
1000
2000
3000
4000
t (s)

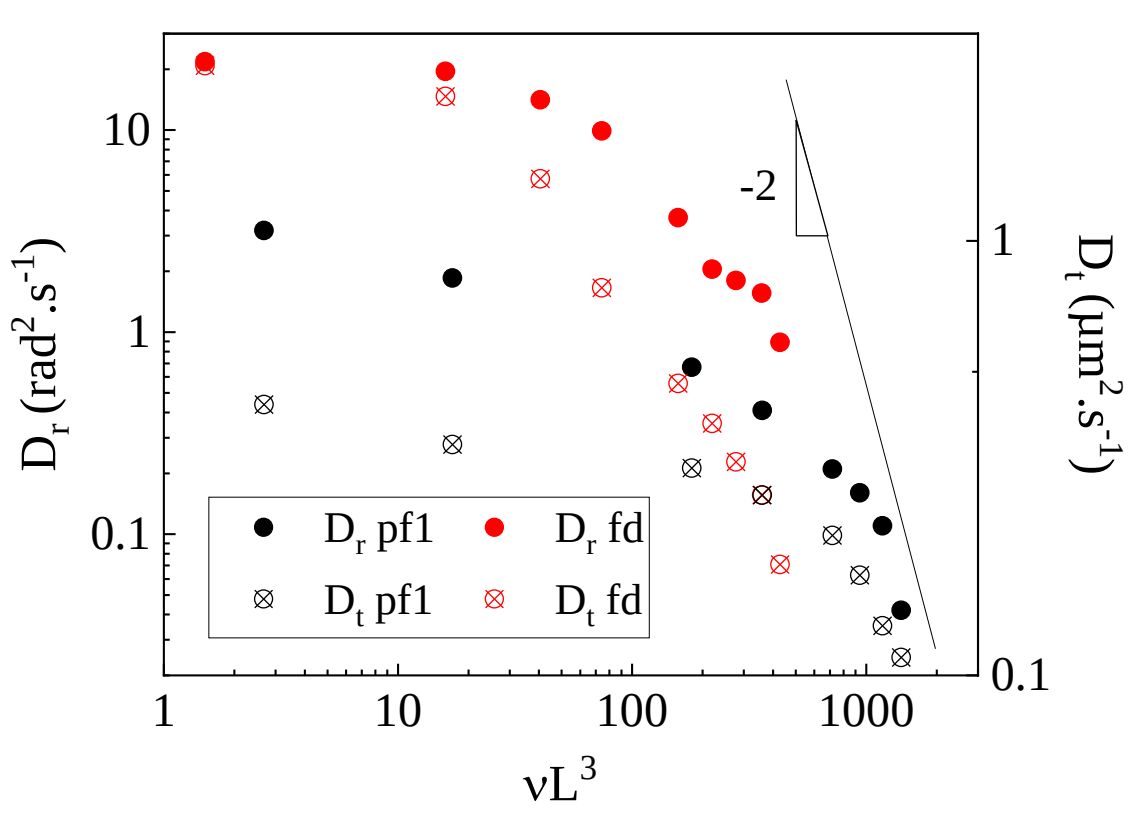
10
1
0.1
D_r (rad^2.s^{-1})
1
0.1
D_t (μm^2.s^{-1})
-2
D_r pf1
D_r fd
D_t pf1
D_t fd
1
10
100
1000
νL^3

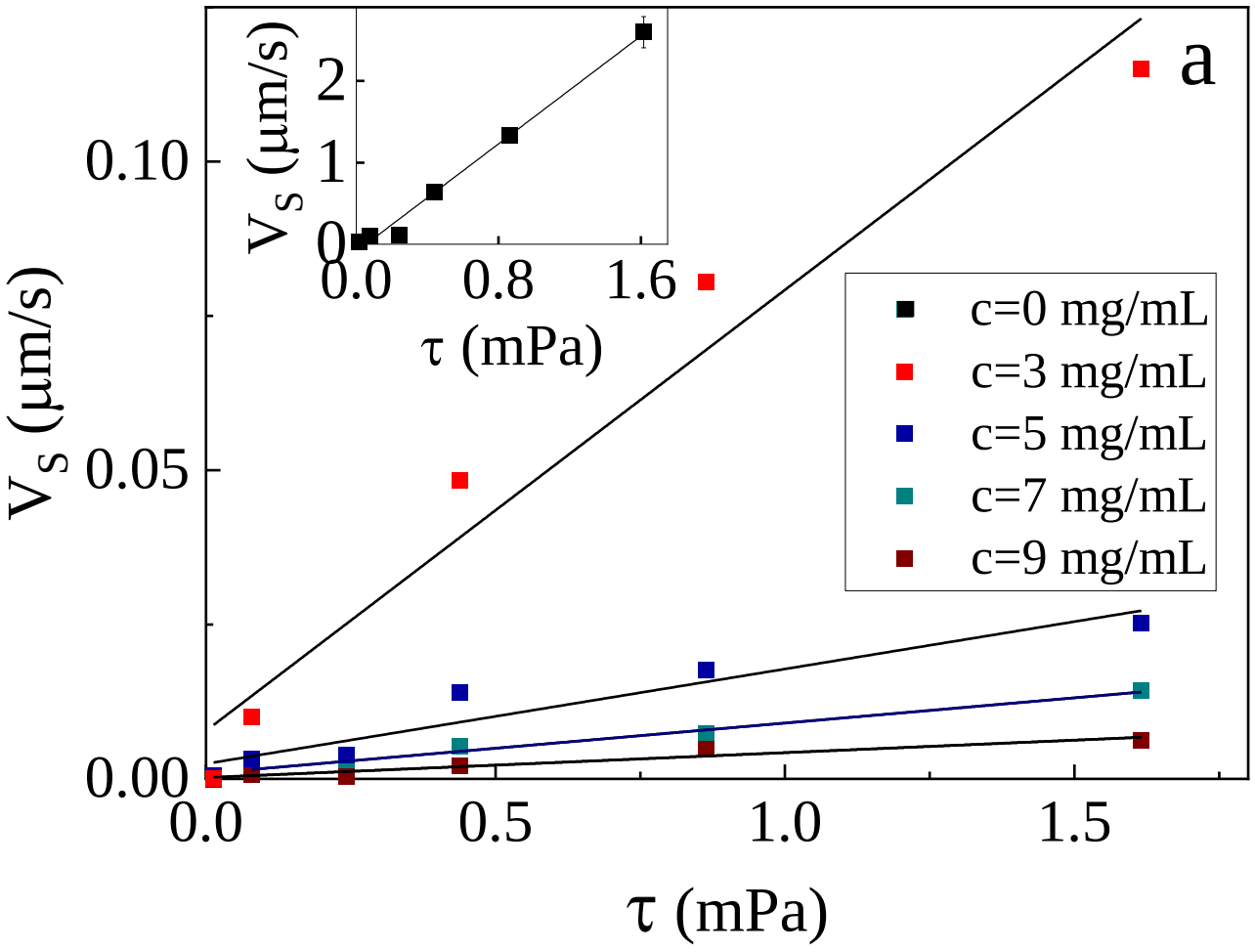
a
V_S (μm/s)
0.10
0.05
0.00
0.0
0.5
1.0
1.5
τ (mPa)
c=0 mg/mL
c=3 mg/mL
c=5 mg/mL
c=7 mg/mL
c=9 mg/mL
V_S (μm/s)
2
1
0
0.0
0.8
1.6
τ (mPa)

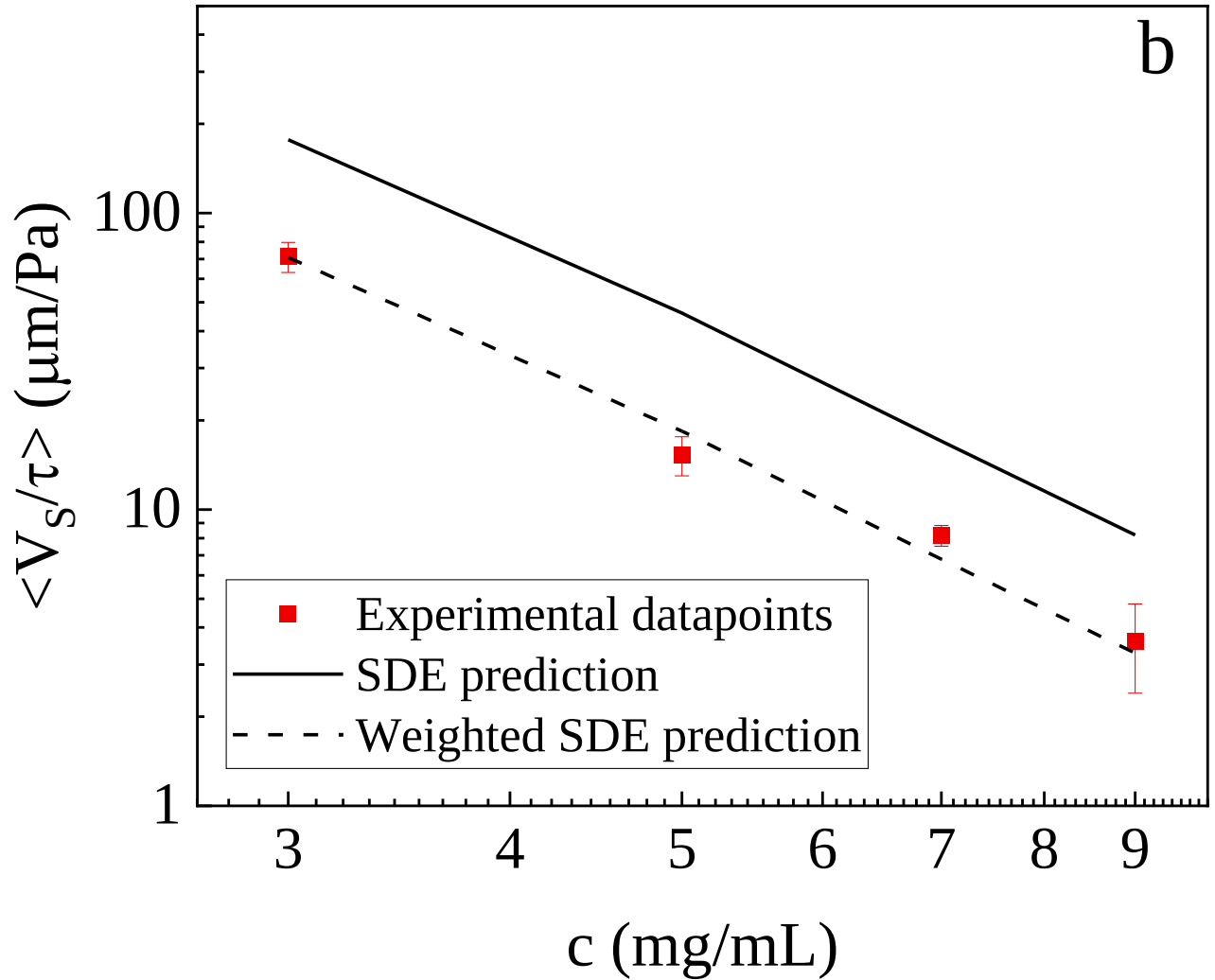
b
$\langle V_S/\tau \rangle$ (μm/Pa)
100
10
1
3
4
5
6
7
8
9
c (mg/mL)
Experimental datapoints
SDE prediction
Weighted SDE prediction

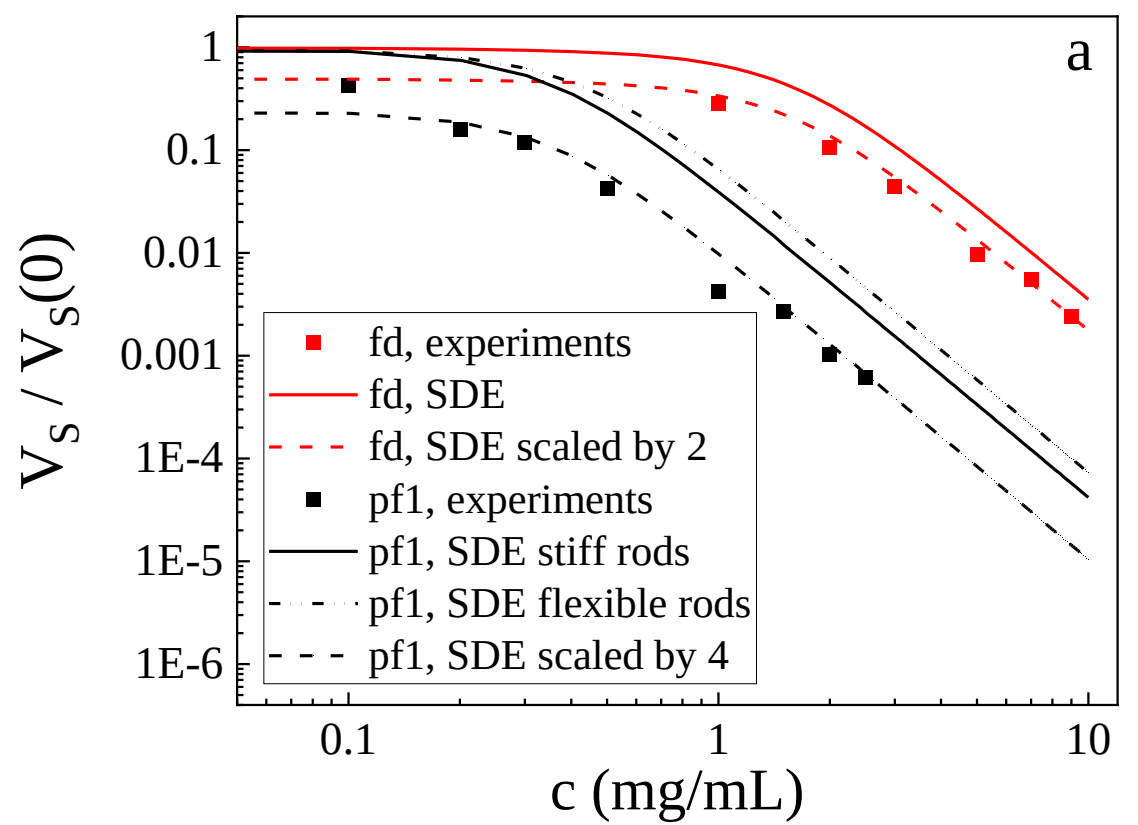
a
1
0.1
0.01
0.001
1E-4
1E-5
1E-6
0.1
1
10
$V_S / V_S(0)$
c (mg/mL)
fd, experiments
fd, SDE
fd, SDE scaled by 2
pf1, experiments
pf1, SDE stiff rods
pf1, SDE flexible rods
pf1, SDE scaled by 4

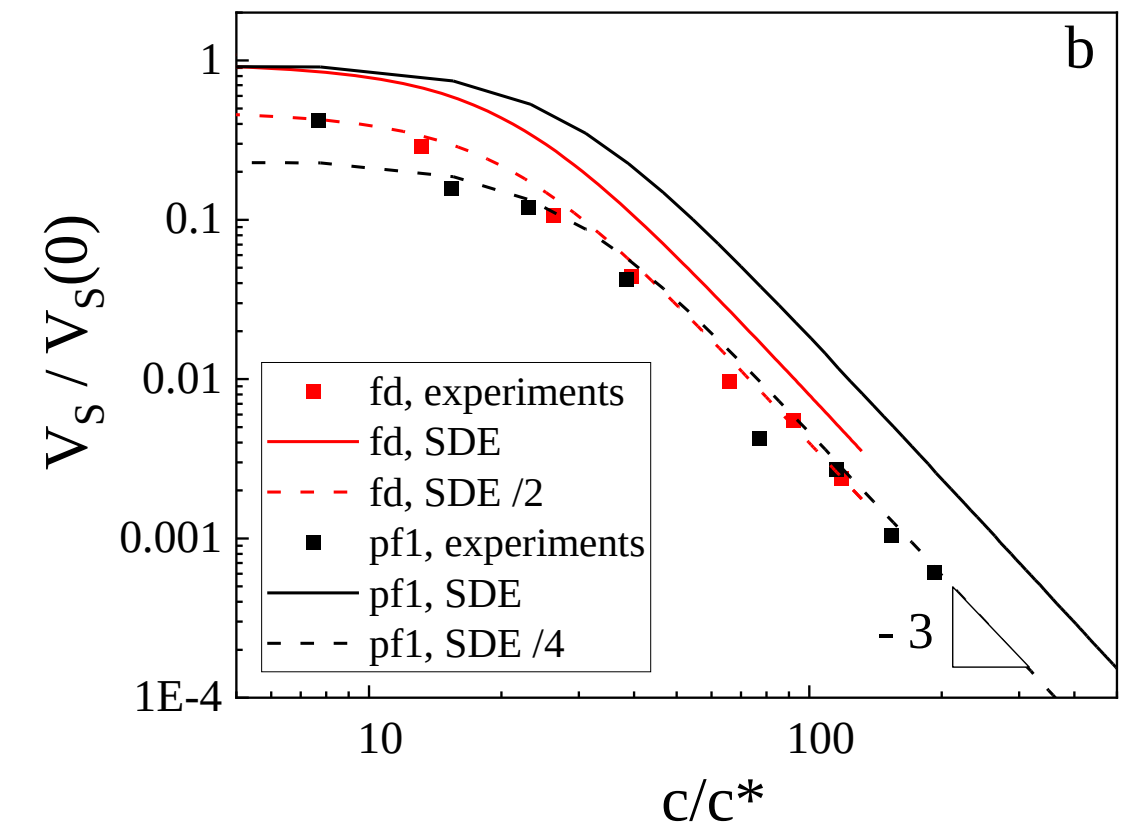
b
1
0.1
0.01
0.001
1E-4
10
100
$V_S / V_S(0)$
c/c*
fd, experiments
fd, SDE
fd, SDE /2
pf1, experiments
pf1, SDE
pf1, SDE /4
- 3

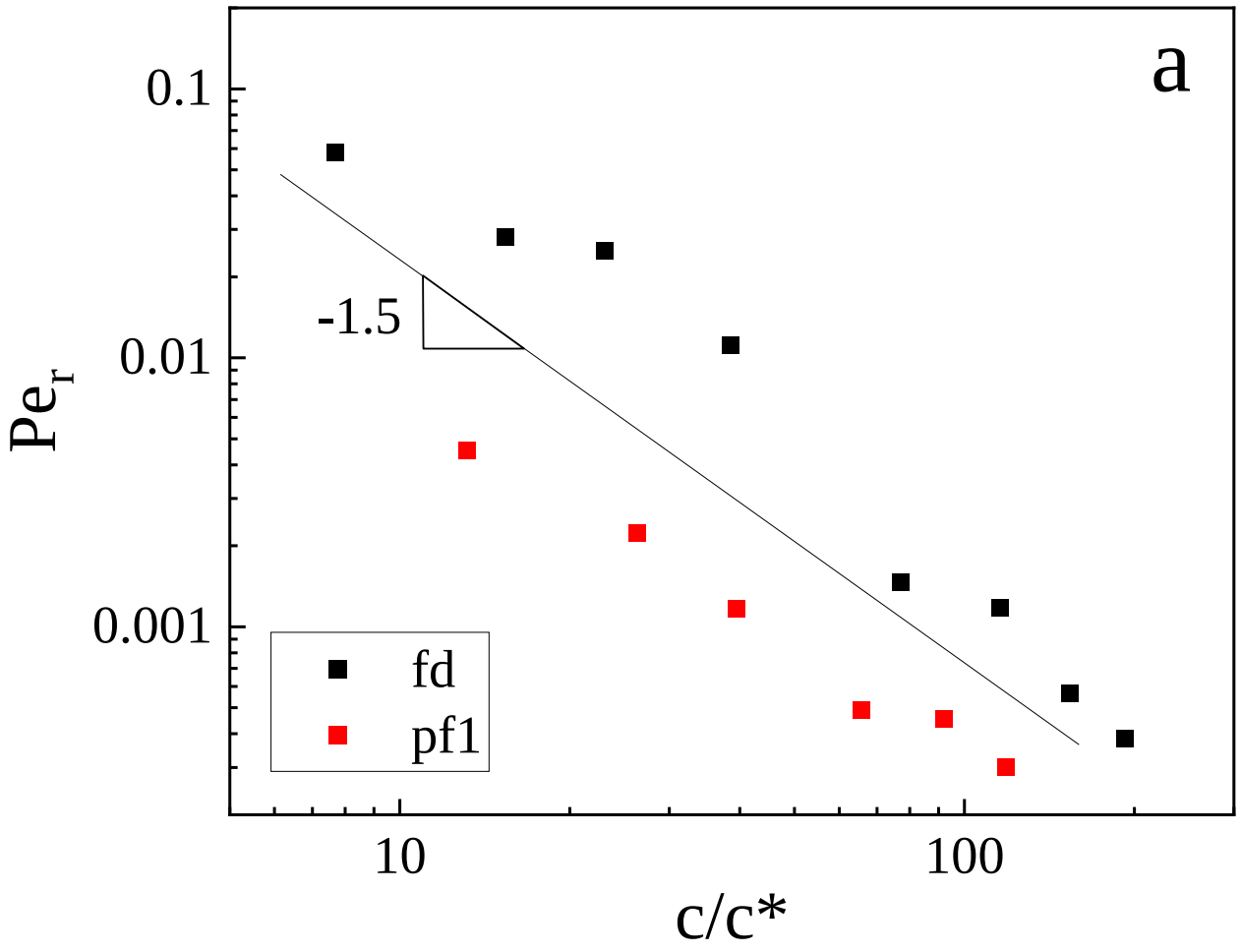
a
0.1
0.01
0.001
Pe_r
-1.5
fd
pf1
10
100
c/c*

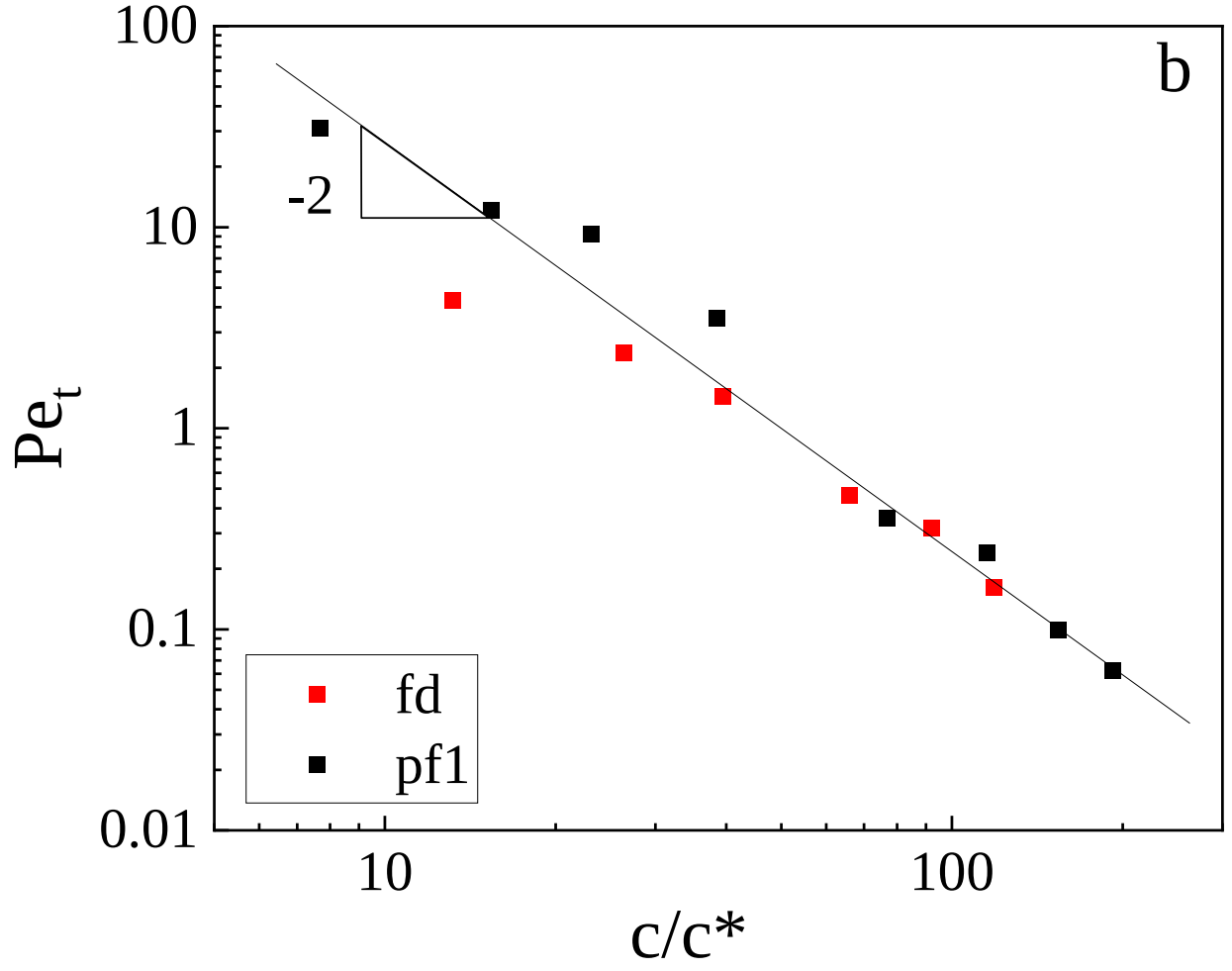
b
100
10
1
0.1
0.01
Pe_t
-2
fd
pf1
10
100
c/c*